Impact of heterogeneous sulfate formation at mineral dust surfaces on aerosol loads and radiative forcing in the Goddard Institute for Space Studies general circulation model

S. E. Bauer and D. Koch

The Earth Institute at Columbia University and NASA Goddard Institute for Space Studies, New York, USA

Received 10 February 2005; revised 21 April 2005; accepted 1 June 2005; published 10 September 2005.

[1] Heterogeneous chemical reactions between sulfate precursors on the surface of mineral dust aerosols affect the atmospheric aerosol cycle and the Earth radiation budget. Heterogeneous reactions of sulfur dioxide with mineral dust particles enhance sulfate formation by producing internally mixed sulfate dust aerosols. The anthropogenic sulfate forcing is estimated to be reduced to -0.18 W/m^2 because of the reduced load of externally mixed sulfate aerosols, compared to -0.25 W/m^2 when heterogeneous surface reactions are excluded. Sulfate coating on mineral dust particles increases wet deposition of dust, causing a positive anthropogenic forcing due to less sulfate coating at preindustrial times. However, heterogeneous reaction pathways are highly uncertain, which is reflected in the wide spread of reaction pathways and uptake probability coefficients in the literature. We undertake a series of sensitivity experiments with the Goddard Institute for Space Studies climate model to investigate the impact of the uncertainty in uptake mechanisms and dust aerosol size distributions on the simulated sulfate cycle. The results of this study are very sensitive to both tested variables. For example, doubling the clay emissions (particles whose radii are less than 1 μm) leads to a sevenfold increase in heterogeneous sulfate production.

Citation: Bauer, S. E., and D. Koch (2005), Impact of heterogeneous sulfate formation at mineral dust surfaces on aerosol loads and radiative forcing in the Goddard Institute for Space Studies general circulation model, *J. Geophys. Res.*, *110*, D17202, doi:10.1029/2005JD005870.

1. Introduction

[2] The amount and chemical composition of aerosol particles have an important influence upon the Earth radiation budget and on climate change. Aerosols impact climate directly, by scattering and absorbing solar radiation and indirectly, by influencing cloud formation, optical properties and lifetime [*Lohmann and Feichter*, 1997; *Menon et al.*, 2002]. Furthermore, many aerosol components, such as sulfates, are air pollutants and can have enduring health impacts. Small particles seem to be especially dangerous because of their ability to travel deeply into the lungs and cause severe health problems [*Brook et al.*, 2002; *Burnett et al.*, 1997].

[3] The role that aerosols play as air pollutants and climate change factors depends strongly on their chemical composition. Aerosols are typically observed to be complex mixtures of chemical species, due to reactions and interactions during transport and cloud processing. Measurements demonstrate that the particle mixing state is highly variable in space and time [*Huebert et al.*, 2003; *Jacob et al.*, 2003]. The result is a complex mixture of several chemical species having radiative properties more complex than those of an externally mixed aerosol population. The radiative properties of aerosols depend upon the size and nature of the mixing of absorbers (such as black carbon and dust) with other common aerosol components such as sulfate, nitrate, organic carbon, sea salt and water. These mixtures range between internal (multiple components within a particle) and external (different components in different particles).

[4] The chemical composition of aerosols is regionally very different. For instance, recent measurement campaigns in the North Pacific (e.g., ACE-Asia [*Huebert et al.*, 2003] and TRACE-P [*Jacob et al.*, 2003]), demonstrate that the majority of aerosol particles are internally mixed in that region [*Ooki and Uematsu*, 2005; *Tang et al.*, 2004; *Jordan et al.*, 2003]. *Trochkine et al.* [2003] analyzed the changing aerosol chemical composition of air masses traveling from China to Japan.

[5] Approximately 40–45% of mineral particles mixed internally with sulfate during their transport in the troposphere. Over Japan mineral particles in the free troposphere were found to be significantly modified as a result of mixing with sulfate, sea salt and anthropogenic contaminants. Particles collected near their source region showed a very small amount of sulfur (about 6%), compared to about 55%

0148-0227/05/2005JD005870$09.00

of particles obtained in the free troposphere over Japan and more than 80% of particles collected in Japan near the ground [*Trochkine et al.*, 2003]. The chemical composition of mineral particles changed as a result of their long-range transport. In contrast, *Putaud et al.* [2004] observed that coarse Saharan dust and fine anthropogenic particles were mainly externally mixed, and no anthropogenic sulfate could be found in the supermicron dust particles. However, during that measurement campaign, Saharan dust was composed primarily of supermicron particles. Sulfate predominately mixes with smaller dust particles, which display a larger surface area per unit mass for chemical reactions.

[6] The observed displacement of fine (submicron) NO_3 toward the aerosol supermicron fraction in the presence of coarse dust particles indicates a significant interaction of HNO_3 with dust [*Putaud et al.*, 2004; *Bauer et al.*, 2004]. In a remote marine environment, observations of boundary layer non-sea-salt sulfate (NSS) aerosols indicate that a substantial NSS fraction is found in coarse (supermicron diameter) sea-salt aerosols [*Sievering et al.*, 2004]. Measurements in southwest Japan showed that sea-salt aerosol change the size and composition of mineral dust, affecting transport, radiative properties and sedimental flux to the oceans [*Zhang and Iwasaka*, 2004].

[7] Aerosol composition is extremely complex. In this work we only focus on the interaction between sulfate and mineral dust aerosols. Previous studies [*Dentener et al.*, 1996; *Liao et al.*, 2003] pointed out the importance of surface reactions regarding the sulfur cycle. *Dentener et al.* [1996] used a global model to study the role of mineral aerosol as a reactive surface and found that 50–70% of sulfate formation is associated with mineral dust. However, the model study focused on the impact of reactive dust surfaces on the chemistry of the troposphere and does not include aerosol feedbacks. *Liao et al.* [2003] investigated aerosol and gas phase chemistry interactions in a climate model. They explained 5% of the global sink of SO_2 by dust uptake, but neglect heterogeneous sulfate production. The impact of air pollution on wet deposition of mineral dust aerosols has been tested by *Fan et al.* [2004]. On the basis of a hypothetical estimate on how SO_2 concentrations affect dust solubility, they infer that air pollution causes an increase of dust deposition to the coastal oceans of east Asia and a decrease in dust deposition in the eastern North Pacific by as much as 50%. *Fan et al.* [2004] simply correlate SO_2 concentrations to dust solubility and thereby neglect many factors that are important for sulfate formation on dust particles, such as ozone or other oxidants, clouds and humidity.

[8] In this article, we calculate the formation of mixed aerosol particles, through heterogeneous surface chemistry using fully interactive models of the sulfate and the dust cycles. This calculation includes the feedback between these cycles and the impact upon radiative forcing.

[9] This study is carried out with the new Goddard Institute for Space Studies (GISS) climate model, called modelE [*Schmidt et al.*, 2005; *Hansen et al.*, 2005]. The model is described in section 2. The sulfate cycle is described and validated by D. Koch et al. (Sulfur species, sea salt and radionuclides in the Goddard Institute for Space Studies modelE, submitted to *Journal of Geophysical Research*, 2005, hereinafter referred to as K05) and previous papers [*Koch et al.*, 1999; *Koch*, 2001]. The model dust cycle is described by R. L. Miller et al. (Mineral dust aerosols in the NASA Goddard Institute for Space Studies ModelE AGCM, submitted to *Journal of Geophysical Research*, 2005, hereinafter referred to as Miller et al., submitted manuscript, 2005) and R. V. Cakmur et al. (Constraining the global dust emission and load by minimizing the difference between the model and observations, submitted to *Journal of Geophysical Research*, 2005, hereinafter referred to as Cakmur et al., submitted manuscript, 2005). In section 3 heterogeneous sulfate formation will be analyzed to discern the impacts on the sulfate and dust cycles and radiative forcing. Heterogeneous surface reactions are highly dependent on parameterizations like gaseous uptake rates or aerosol size distributions. A series of sensitivity experiments is discussed in section 3.4 to test the robustness of the results discussed in this paper. Final conclusions are drawn in section 4.

2. Model Description

[10] Results from the Goddard Institute for Space Studies (GISS) general circulation model (GCM) are presented for present-day (circa 2000) and preindustrial (circa 1750) simulations. The ModelE version of this code is a complete rewrite of previous models incorporating numerous improvements in basic physics, the stratospheric circulation and forcing fields [*Schmidt et al.*, 2005]. Most notably the model top has been raised to the stratopause near 0.1 hPa, and the number of vertical layers was increased from 12 to 20. The model follows a Cartesian grid point formulation for all quantities. The employed horizontal resolution amounts to $4^\circ \times 5^\circ$ latitude by longitude. The model uses a 30 minute time step for all physics calculations. A complete model description is given by *Schmidt et al.* [2005].

[11] The GCM carries externally mixed aerosol mass, including sulfate, sea salt (and radionuclide tracers) (K05), carbonaceous aerosols (with distinction between biomass and anthropogenic BC and OC) [*Koch and Hansen*, 2005], and dust [*Cakmur et al.*, 2004; Miller et al., submitted manuscript, 2005; Cakmur et al., submitted manuscript, 2005] The sulfate and sea salt model as well as the tracer transport scheme is described and validated in detail by K05.

2.1. Surface Reactions on Mineral Dust Aerosols

[12] Mineral dust is the largest component, in terms of mass, of airborne particulate matter in the global atmosphere [*Andreae*, 1995]. Close to source regions, e.g., the Sahara or the Gobi desert, the area of mineral aerosol surface is estimated to be equivalent to up to 30% of the Earths surface [*Dentener et al.*, 1996; *Bauer et al.*, 2004]. With a lifetime of several days to weeks for the smallest dust particles, desert dust is widely spread over the globe and provides a surface for heterogeneous reactions. Field studies in remote and continental regions have shown that mineral dust particles are often coated with sulfates and nitrates [*Savoie and Prospero*, 1982; *Savoie et al.*, 1989, 1994; *Levin et al.*, 1996; *Zhuang et al.*, 1999; *Zhang et*

al., 2000]. The mixing state and the impact of desert dust on aerosol formation was one important focus during the ACE-Asia campaign [*Huebert et al.*, 2003].

[13] In this publication we are particulary interested in the uptake of SO_2 on mineral surfaces, because this affects the formation of sulfate aerosols and the hygroscopicity of mineral dust.

[14] The reaction mechanism of SO_2 oxidation to form sulfate on mineral dust is assumed to proceed via two major steps [*Ullerstam et al.*, 2002]: First, SO_2 is reversibly absorbed on the dust surface followed by a second, irreversible reaction in which absorbed SO_2 is oxidized to sulfate by ozone.

[15] To our knowledge, only a few laboratory studies exist that measure the heterogeneous uptake and oxidation of SO_2 on mineral dust. *Usher et al.* [2002, 2003] measured the uptake of SO_2 on a range of mineral oxide compounds as well as authentic dust samples in a Knudsen cell reactor. They found that SO_2 is irreversibly absorbed as sulfite (SO_3^{2-}) and bisulfite (HSO_3^-) on the mineral particles, with initial uptake coefficients ranging from 10^{-7} (for SiO_2) to 10^{-4} (for MgO). The uptake coefficients for $CaCO_3$ and China loess were observed to be in the range of 10^{-4} and 10^{-5}, respectively.

[16] A diffuse reflectance infrared Fourier transform spectroscope (DRIFTS) was used by *Ullerstam et al.* [2002], and they found that the uptake coefficient for SO_2, $\gamma_{(SO_2)}$, is independent of the ambient SO_2 concentration. $\gamma_{(SO_2)}$ is determined to be on the order of $\gamma_{(SO_2)} = 10^{-3}$ to $\gamma_{(SO_2)} = 10^{-7}$.

[17] In all experiments surface saturation was observed with an amount of 2×10^9 sulfate ions g^{-1} on the mineral dust sample. In the presence of water vapor regeneration of active sites was observed. After repeated exposure to water vapor corresponding to 80% relative humidity and successive SO_2 and O_3 treatments, the amount of sulfate covering the surface was increased by 47% compared to the dry experiments.

[18] Guided by these publications, we chose the uptake coefficients of $\gamma_{SO_2} = 10^{-4}$ for humidity larger than 60% and 10^{-7} for dryer conditions.

[19] The following equations are used in modelE to describe the gas uptake on dust surfaces: The net removal of gas-phase species j to an aerosol surface is described by k_j (s^{-1}) a pseudo first-order rate coefficient:

$$k_j = \int_{r^2}^{r^1} k_{d,j}(r) n(r) dr \tag{1}$$

where $n(r)dr$ (m^{-3}) is the number density of particles between the aerosol radius interval r and $r + dr$. $k_{d,j}$ describes the size-dependent mass transfer coefficient (m^3/s) calculated using the equation [*Fuchs and Sutugin*, 1970]

$$k_{d,j} = \frac{4\pi r D_j V}{1 + K_n\left(\lambda + 4\dfrac{(1-\gamma_j)}{3\gamma_j}\right)} \tag{2}$$

where D_j is the gas-phase molecular diffusion coefficient of a trace gas in air (m^2/s) [e.g., *Chapman and Cowling*, 1970; *Davis*, 1983]:

$$D_j = \frac{3}{8Ad_q^2\rho_a}\sqrt{\frac{R^\star T m_a}{2\pi}\left(\frac{m_q + m_a}{m_q}\right)} \tag{3}$$

where A is Avogadro's number, ρ_a the density of air, $R^\star$ the gas constant, T the temperature, m_a and m_q the molecular weight of air and gas q, d_q is the diameter of the gas molecule ($\approx 4.5\dot{A}$). Further variables used in equation (2) are the ventilation coefficient V (set to unity in our experiments), K_n the Knudsen number, λ is the effective free pathway of a molecule in air, and γ_j, the uptake coefficients of a gas on aerosol surfaces as determined by the laboratory studies.

[20] This gaseous uptake process is followed by an oxidation process. The sulfur that is deposited on the dust surface is oxidized by ozone following *Maahs* [1983] and *Shure et al.* [1995], using off-line ozone fields from *Bell et al.* [2005].

[21] We are aware that uptake rates are extremely difficult to measure and because these rates are crucial to the results discussed in this paper we performed a series of sensitivity studies where we tested different uptake rates. The results are described in section 3.4. We would like to mention that former global modeling studies [*Dentener et al.*, 1996; *Liao et al.*, 2003] used much higher uptake rates, ranging from 0.1 to 3×10^{-3} depending on the relative humidity of the air mass.

2.2. Sulfate Cycle

[22] We briefly summarize the model sulfur cycle here and refer to K05 for details. Sulfur species include DMS, SO_2 and sulfate, along with a semiprognostic H_2O_2 needed for aqueous phase oxidation. DMS emissions are based upon DMS water concentrations [*Kettle et al.*, 1999] and the sea-air transfer function of *Nightingale et al.* [2000]. The industrial SO_2 emission is from IIASA (International Institute for Applied Systems Analysis; F. Dentener, manuscript in preparation, 2004; M. Amann, personal communication, 2004). The SO_2 emission from continuous volcanic venting is based on the GEIA volcanic emissions [*Andres and Kasgnoc*, 1998]. However, these are increased by a factor of 1.5 according to recent estimates [e.g., *Halmer et al.*, 2002; *Graf et al.*, 1997].

[23] The species are transported using the quadratic upstream scheme [*Prather*, 1986]. Gas phase chemistry includes oxidation of SO_2 by OH, formation and destruction of H_2O_2 and oxidation of DMS. H_2O_2 is treated semiprognostically, and we use input fields to generate and remove H_2O_2 (its photolysis rate, HO_2, and OH). These fields (also NO_3 needed for DMS oxidation) are now taken from the modelE gas chemistry [*Bell et al.*, 2005]. These are based on monthly mean 3D fields. Dry deposition uses a resistance-in-series scheme and includes gravitational settling. Aqueous phase oxidation (of SO_2 by H_2O_2) and uptake and removal by stratiform and convective clouds are coupled to cloud processes (including condensation, transport, entrainment, detrainment, updraft transport, autoconversion, evaporation and impaction by raindrops).

Table 1. Global Annual Sulfur Budget

	K05, Tg S	This Work: EXP, Tg S	EXP – K05, %
	Base Case I		
SO_2	0.66	0.46	−32
SO_4 total	0.48	0.50	+3
SO_4 externally mixed	0.48	0.37	−24
	Sensitivity Experiment II		
SO_2	0.67	0.42	−37
SO_4 total	0.46	0.56	+20
SO_4 externally mixed	0.46	0.31	−33

2.3. Mineral Dust

[24] The upgraded mineral dust parameterization in modelE is described more completely and compared to observations by Miller et al. (submitted manuscript, 2005). Global emission were derived to maximize the resemblance of the model dust cycle to a global array of observations ranging from satellite and Sun photometer retrievals of aerosol optical thickness to in situ measurements of surface concentration and deposition and size distribution (Cakmur et al., submitted manuscript, 2005). Emission occurs in regions identified by *Ginoux et al.* [2001] as "preferred sources," which are arid basins where abundant particles susceptible to erosion accumulate from fluvial erosion of the surrounding highlands [*Prospero et al.*, 2002]. It is assumed that dust is emitted when the surface wind speed exceeds 8 m^{-1}. Within each grid box, a probability distribution of wind speed is calculated that depends both upon the resolved value explicitly calculated by the AGCM and subgrid fluctuations associated with boundary layer turbulence, dry convective thermals and moist convective downdrafts [*Cakmur et al.*, 2004].

[25] In this paper two different types of dust emissions are used: Prescribed dust emissions after *Ginoux et al.* [2005, 2001] (http://nansen.ipsl.jussieu.fr/AEROCOM/) and the interactive dust emission sources as described above. Prescribed dust emissions are used in this study to exclude feedbacks with the uplift of dust particles, which would complicate the interpretation of the results when comparing the various experiments. However, that might be in conflict with the models meteorology. Dust particles are represented by four size classes: 0.1–1 (clay), 1–2 (silt1), 2–4 (silt2), 4–8 (silt3) μm. The global dust emission of the prescribed sources is 1546 Tg/yr, where 154 Tg/yr are emitted as clay particles, and 448 Tg/yr, 612 Tg/yr and 332 Tg/yr are emitted as silt particles, respectively. The different dust particle classes provide the surface area for the production of sulfate as described in section 2.1. We assume a lognormal distribution in each dust size class to calculate the number distribution. The surface area of each particle is calculates by assuming spherical particles, which might underestimate the actual surface area. The formation of sulfate on dust leads to a coated particle, having a mineral core that is partly or completely coated by sulfate. The fractional sulfate coating of dust determines the solubility of the mixed particle. Pure sulfate aerosols are completely soluble, while pure dust particles are assumed to be insoluble. In our model, we assume that a dust particle with 10% of its surface coated by sulfate is completely soluble. This value is taken from *Wyslouzil et al.* [1994] and *Lammel and Novakov* [1995], who discuss hydration effects of aerosols. However, this value has not been measured explicitly for coated mineral dust particles. Dust solubility is set to a constant value of 0.5 in the control simulations, where dust surface reactions are not included. Below-cloud scavenging still occurs for insoluble particles. We implicitly assume large impaction effects in moist convective clouds with 50% of insoluble particles scavenged in convective updrafts. The effect of solubility of coated particles upon dust removal rates is given in section 3.2.

3. Experiment

[26] The impact of heterogeneous reactions on global aerosol cycles and climate is analyzed by comparing two simulations: A control simulation where no interactions between SO_2 and mineral dust aerosols are considered (hereinafter referred to as K05) and an experiment where dust surface reactions are included (hereinafter referred to as EXP). The sulfate simulation in K05 is similar to the simulation as discussed by K05, but in this work we also include dust tracers, using the prescribed emissions, so that we have a control case without heterogeneous chemistry for both aerosol classes (sulfate and mineral dust). The simulations are run for six years and the last five years are averaged. We simulate both present-day (with year 2000 emissions, including anthropogenic sources) and preindustrial (year 1750, with natural emission only) aerosol burden.

3.1. Impact of Dust on the Sulfate Cycle

[27] The heterogeneous sulfate formation on the dust particles uses SO_2 and O_3 as precursor species. This additional reaction pathway leads to an enhanced oxidation of SO_2, which leads to reduced ambient SO_2 concentrations. K05 has discussed that their model strongly overestimates the observed SO_2 concentrations, especially in polluted regions, for example when compared to the European EMEP station network (K05, Figure 6). In the current simulation, the global annual mean budget for SO_2 is reduced from 0.66 Tg S to 0.46 Tg S (see Table 1), because of surface reactions on dust. Figure 1 shows the SO_2 concentrations in the near-surface layer, at 500 hPa height, and as a zonal mean, for the EXP simulation and for the difference of EXP with respect to K05. The largest reduction in SO_2 concentrations occurs in the Northern Hemisphere, in high latitudes in the lower troposphere. Figure 1 (upper right panel) shows that the areas with the highest concentration reductions are located in east Asia, eastern Europe and western Russia. The zonal mean plot (see Figure 1) shows that the largest reduction in SO_2 concentration occurs in the polar latitudes, indicating a reduced polar transport of SO_2 molecules due to increased SO_2 oxidation.

[28] In comparison to the European surface observations network (EMEP), the current simulation shows an improvement, but still overestimates strongly the observed SO_2 concentrations. The root mean error improves from 0.3 to 0.5, for the K05 and the EXP simulation, respectively, and the mean concentrations drop from 2.3 (K05) to 1.7 ppb_v (EXP), still overestimating strongly the observed European surface concentrations which show a mean concentration of 0.8 ppb_v. The vertical distribution of SO_2 concentration is

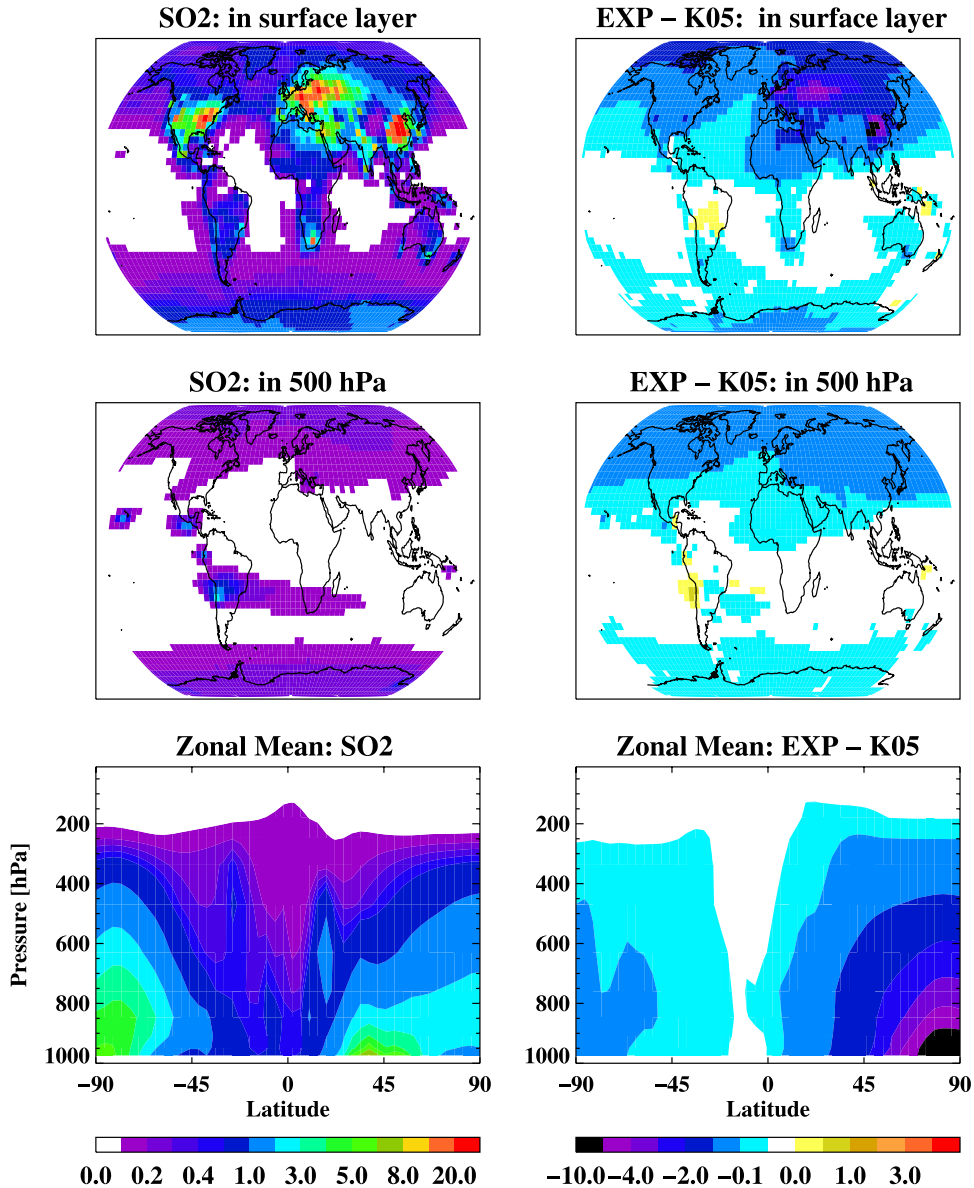

Figure 1. (left) Annual mean SO_2 concentration at the surface, at the 500 hPa layer, and as zonal mean and (right) concentration differences between EXP and K05. Units are $\mu g/m^3$.

compared to measured SO_2 profiles in Figure 2, with simulated monthly mean SO_2 concentrations interpolated to the flight track. Observations are shown for the TRACE-P [*Jacob et al.*, 2003], PEM-West B [*Hoell et al.*, 1997] and PEM-Tropics campaign [*Dibb et al.*, 2002]. TRACE-P took place in the spring of 2001 covering the Pacific ocean, PEM west B focused on the western Pacific and took place in spring 1994, and PEM-Tropics took place in the tropical Pacific in spring 1999. Figure 2 shows that the reduced SO_2 concentration in the free troposphere of the current simulation (EXP) seems to better match the observed value. However, in general, SO_2 tends still to be overpredicted in the model, so even more oxidation mechanisms removing SO_2 are needed.

[29] The sulfate produced in the simulation exists in two different forms, as pure externally mixed sulfate particles and as sulfate that is internally mixed with dust particles, i.e., coated to the dust surface. Figure 3 shows the total sulfate burden along with pure (externally mixed) and internally mixed components. The horizontal distribution of the pure sulfate mass shows a maximum concentration over the northern African continent. This distribution resembles the sulfate distribution in K05 but with a reduced amplitude. The sulfate burden in K05 is 0.48 Tg S. If we compare only the pure sulfate aerosols with each other (in K05 all sulfates are pure sulfates) then the pure sulfate burden is reduced by 24% to 0.37 Tg S in EXP. Nonetheless, the total sulfate burden is increased (0.5 Tg S) in the EXP simulation by 3% compared to K05 (see Table 1). The total sulfate burden is increased because of the sulfate material that coats the individual dust particles. Nearly all of this sulfate is present over the continents in the Northern Hemisphere, with maximum concentrations in east Asia and southeast Europe, Arabia, and northern Africa.

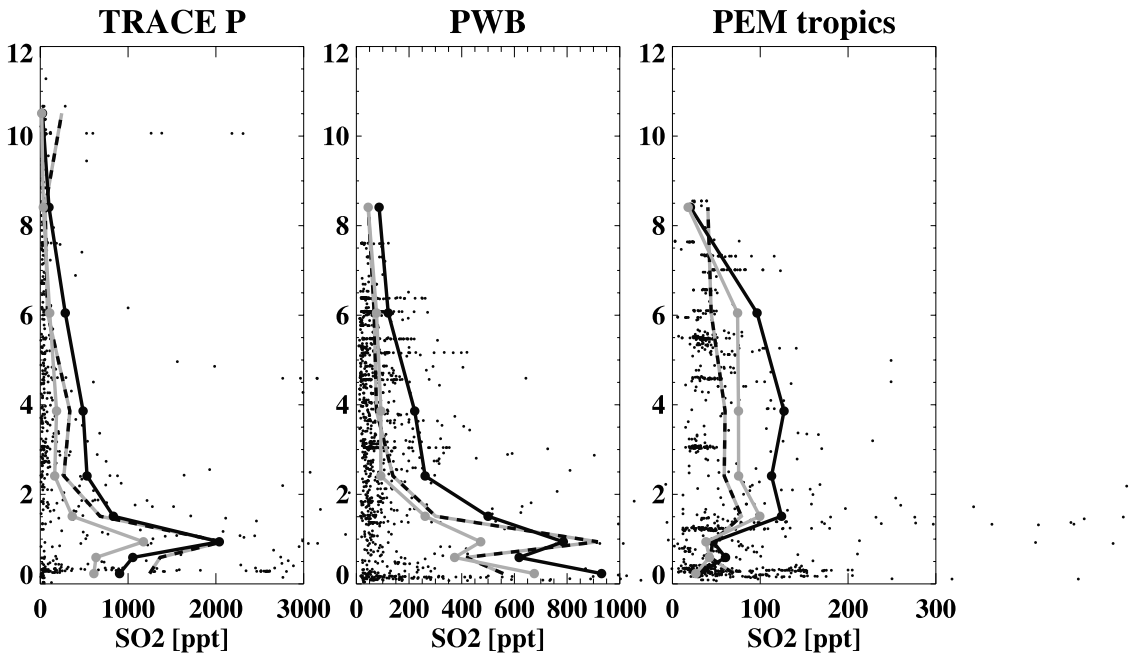

Figure 2. Comparison of model (grey lines, EXP; black lines, K05) with aircraft (grey-and-black dashed lines) profiles of SO_2 concentrations. The black points represent single aircraft measurements. The vertical axis is altitude in kilometers, and the concentration units are pptv. Profiles are constructed by using the model values at the locations corresponding to each observation and then averaging all model and observed values.

[30] Comparing the changes in SO_2 and SO_4 concentrations, we find that much more SO_2 is oxidized (32% more gets lost compared to K05), but total sulfate production is only increased by 3%. This can be explained by the faster removal of internally mixed aerosols, and therefore a changed lifetime of sulfate. However, this result depends strongly on the life cycle and especially the size distribution of dust. This problem will be addressed in the sensitivity experiments described in section 3.4.

[31] Figure 4 shows that in the near-surface layer, the largest contribution from surface reaction on dust to the sulfate burden appears in Eurasia, with large contributions in the polluted regions in the Northern Hemisphere like eastern Europe and east Asia. In contrast to this increased load close to the surface, sulfate is reduced in the free troposphere (Figure 4). Because of the large surface signal over Europe and USA, a comparison to the EMEP and IMPROVE sulfate measurements is shown in Figure 5. Scatterplots between the simulated (EXP and K05) and the EMEP and IMPROVE observations are shown for the annual mean and separately for the summer and winter months. The correlation coefficient between monthly averaged observations and simulations increases from 0.74 (K05) to 0.82 (EXP) for the IMPROVE comparison and from 0.45 (K05) to 0.76 (EXP) for EMEP. The additional sulfate produced through dust surface reactions improves the simulation of high sulfate concentrations especially in the winter season.

[32] The largest impact of heterogeneous sulfate production occurs over east Asia (Figure 4). Figure 6 compares the

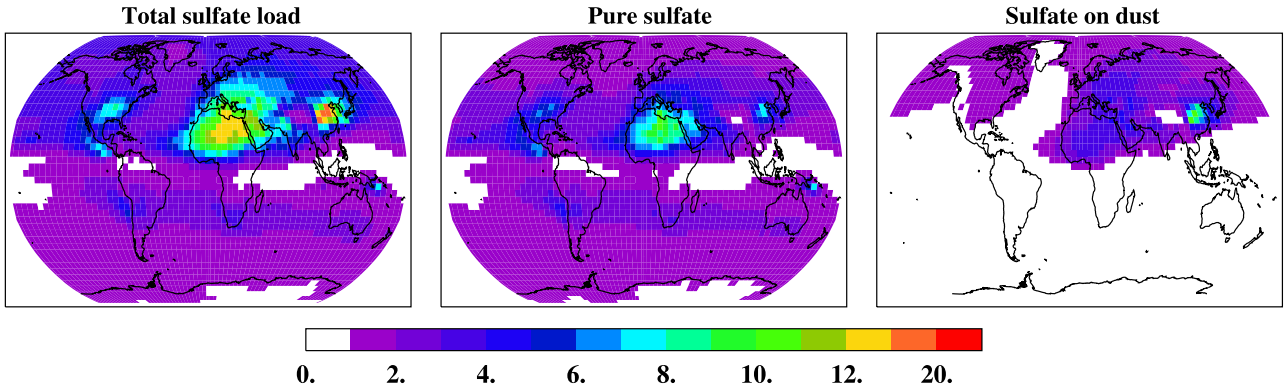

Figure 3. (left) Annual mean column loads of sulfate, and its contributions as (middle) pure sulfate and (right) sulfate coated upon dust. Units are mg/m^2.

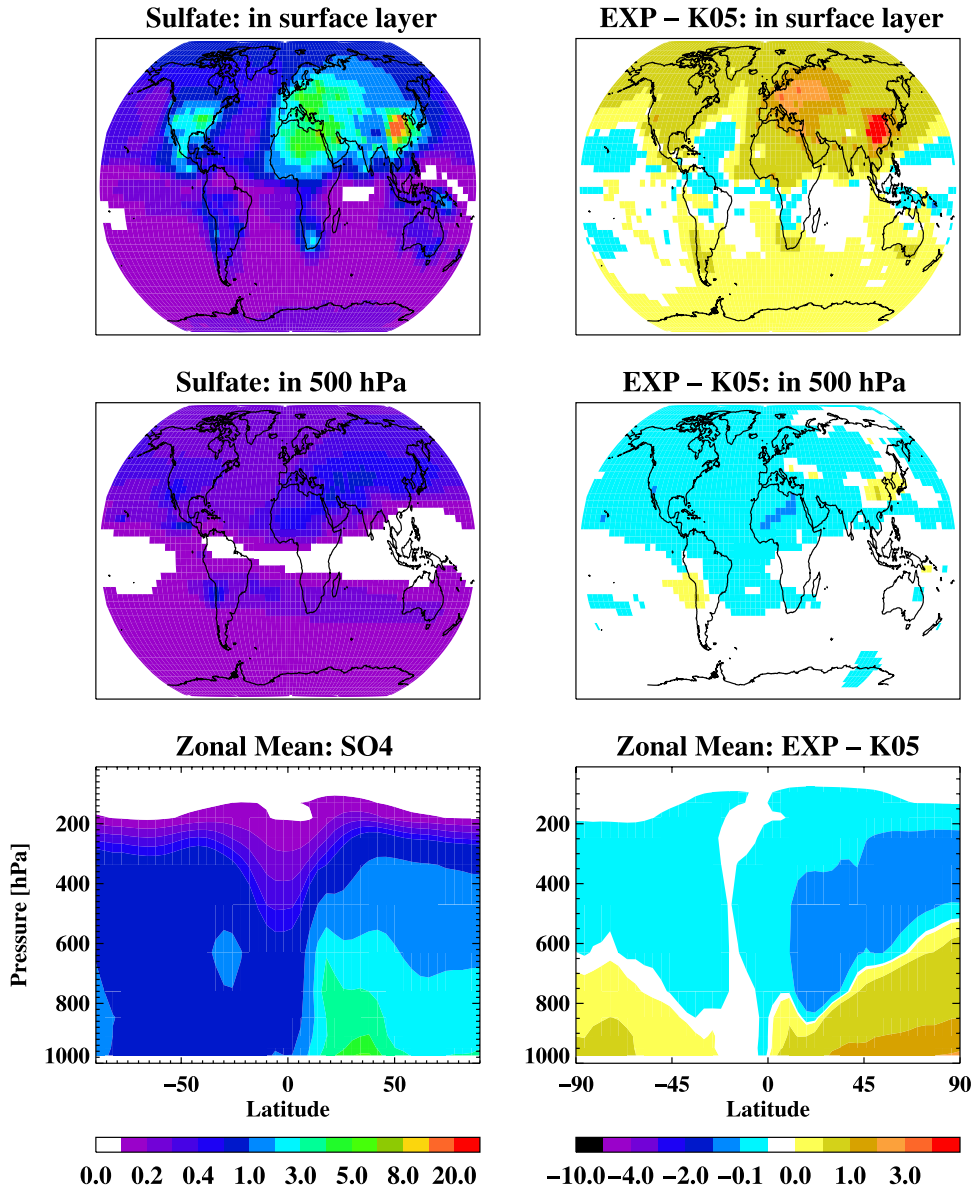

Figure 4. (left) Annual mean sulfate concentration at the surface, at the 500 hPa layer, and as zonal mean and (right) concentration differences between EXP and K05. Units are $\mu g/m^3$.

simulations (EXP and K05) to aircraft measurements during ACE-Asia, TRACE-P and PEM-Tropics. The measurements during ACE-Asia were taken in spring 2001, following the pollution downwind of east Asia over the Pacific Ocean. In general, the increased sulfate concentration in EXP improves the comparison, but the observed profiles show even higher sulfate concentrations. In case of ACE-Asia, sulfate is increased by more than 100% in the planetary boundary layer (PBL) compared to K05. TRACE-P, which observed the same region as ACE-Asia, but over a larger region of the Pacific Ocean, show much higher sulfate concentrations in the PBL compared to the model. These high observed sulfate concentrations in the marine boundary layer could indicate that sulfate is mixed with sea salt particles in these areas. The heterogeneous uptake and sulfate formation process within sea salt particles is not yet included in the model. The same situation is seen in the PEM-Tropics profile, which also measured air masses that have traveled far over maritime regions.

[33] The data set of D. Savoie and J. Prospero (personal communication, 1999) is a valuable source of information about aerosol background concentrations. At most stations EXP performs better than K05 in these remote regions (not shown), but stations with high sulfate and dust concentration are of special interest. Figure 7 shows two Asian stations where high dust concentrations are observed: Cheju in Korea and Okinawa, Japan. At both sites sulfate concentrations increase by more than 100% during spring time, the high-dust season in Asia, but still show lower concentrations compared to the observations.

3.2. Impact on the Dust Cycle

[34] Sulfate coating on dust aerosols impacts the solubility of the dust particles and therefore influences the wet

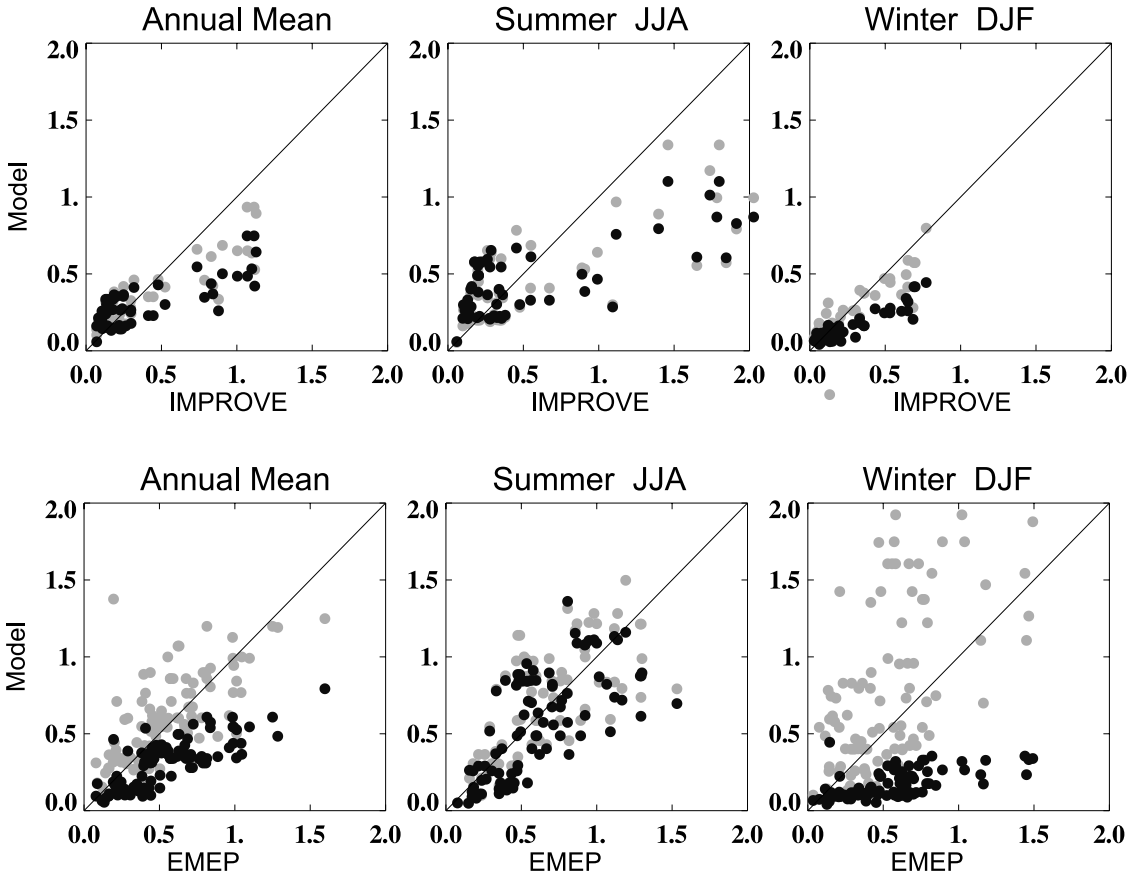

Figure 5. Scatterplots of observed and modeled (black points, K05; grey points, EXP) sulfate concentrations for (top) the U.S. American IMPROVE network and (bottom) the European EMEP network. Annual mean and summer and winter conditions are shown separately. Units are ppbv.

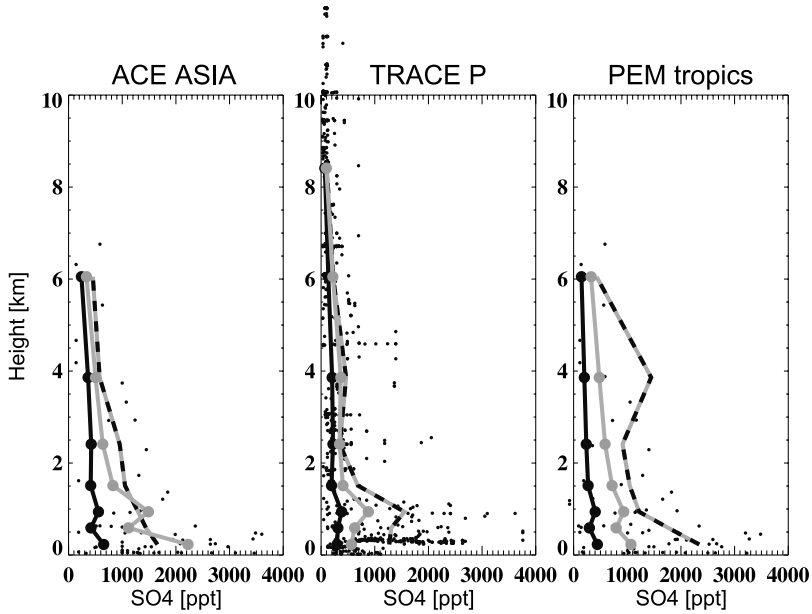

Figure 6. Comparison of model (grey lines, EXP; black lines, K05) with aircraft (grey-and-black dashed lines) profiles of sulfate concentrations. The black points represent single aircraft measurements. The vertical axis is altitude in kilometers, and the concentration units are pptv. Profiles are constructed by using the model values at the locations corresponding to each observation and then averaging all model and observed values.

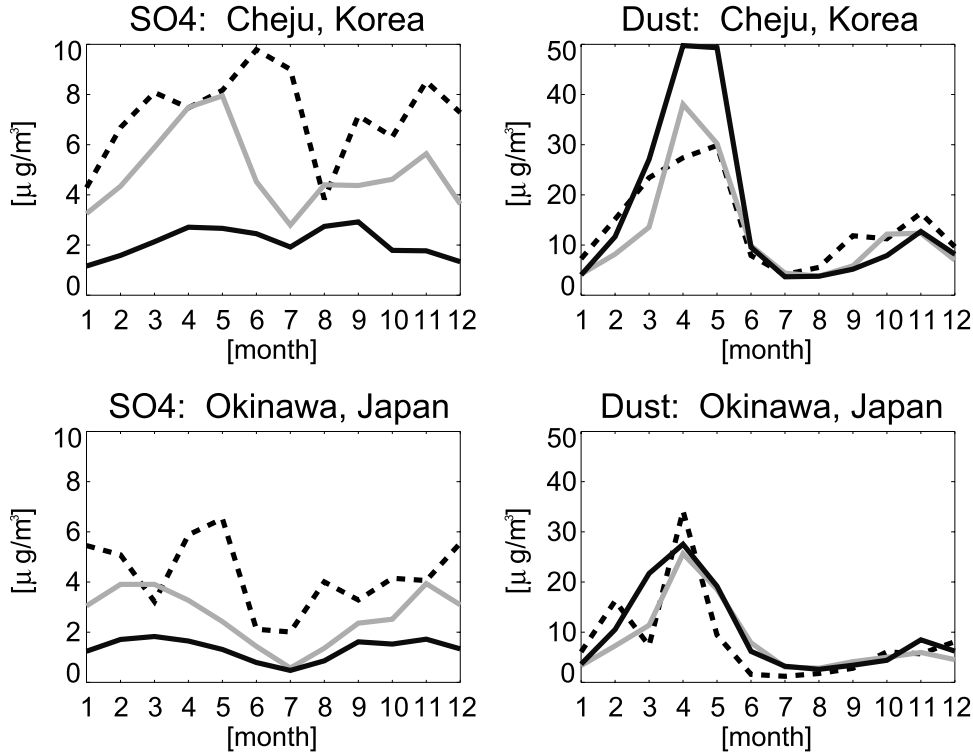

Figure 7. Time series of modeled (solid grey lines, EXP; solid black lines, K05) and observed (dashed lines) (left) sulfate and (right) dust aerosol volume concentrations at two Asian measurement sites, Cheju in Korea (upper panels) and Okinawa in Japan (lower panels). The concentrations are given in $\mu g/m^3$.

removal rate. The time series (Figure 7) at Cheju and Okinawa show that heterogeneous sulfate uptake in EXP is associated with a slight reduction in mineral dust load compared to K05 during the high-dust season.

[35] In this study we look at the impact of increased solubility upon aged dust particles. However, the size of this effect depends on the assumption that is made for the solubility of the non sulfate coated particles. Table 2 summarizes the results of a series of sensitivity tests, where the solubility of mineral dust was varied. The following cases were tested: (a) Mineral dust is insoluble, (b) it has a solubility coefficient of 0.5, (c) it is completely soluble, (d) its solubility depends on the sulfate surface coating. Table 2 also gives the budgets for the four different size classes. The difference between load and lifetime for the two most extreme cases lies between 21 and 29 Tg and 4.9 and 6.8 days, respectively. Both of these values are still in the middle range of estimated atmospheric dust loads and lifetimes [*Zender et al.*, 2004].

[36] In case of the coated particles, case d, we assume that a mineral dust particle becomes completely soluble when 10% of the particle surface is covered by sulfate. We assume that 10% of the dust surface is coated when enough sulfate material is collected by a core dust particle to form a shell around the whole particle which has the thickness of 1% of the core particle diameter. In addition, we assume that particles without a sulfate coating still have a solubility coefficient of 0.5. This assumption is made to account for non sulfate coatings, for example nitrate, that can impact the solubility of the mineral dust particles as well. The annual mean dust budget (Table 2) of case d is close to the budget of case b. Most of the sulfate that is coated to dust sticks to the clay dust particles; this is the smallest size class in our model. Forty-eight percent of the sulfate material coats clay particles, 43% coats Silt1, and 8% Silt2. Particles larger than 2 μm experience negligible sulfate coating. Large particles have a short lifetime and provide only a small surface area for heterogeneous reactions, whereas clay

Table 2. Global Annual Mineral Dust Budget[a]

Experiment	Loads, Tg	Wet Deposition, Tg/yr	Turbulent Deposition, Tg/yr	Sedimentation, Tg/yr	τ	Lifetime, days
Insoluble dust[b]	29 (7/13/8/1)	379 (84/176/110/9)	369 (64/148/129/28)	798 (6/124/373/295)	0.028	6.8 (14/10/5/1)
Constant solubility[c]	24 (5/11/7/1)	422 (89/193/128/12)	347 (59/137/123/28)	777 (6/118/361/292)	0.021	5.6 (11/8/4/1)
Soluble dust[d]	21 (4/9/7/1)	461 (94/206/146/15)	330 (55/129/118/28)	755 (5/113/348/289)	0.018	4.9 (8/7/4/1)
Coated dust[e]	23 (5/10/7/1)	433 (92/200/132/13)	338 (56/133/121/28)	771 (6/115/359/291)	0.02	5.5 (9/7/4/1)

[a]Values in parentheses indicate partitioning into clay and the three silt classes (C/S1/S2/S3).
[b]Solubility is set to zero.
[c]Solubility coefficient is set to 0.5.
[d]Particles are completely soluble.
[e]Particles are completely soluble when 10% of the surface is coated by sulfate.

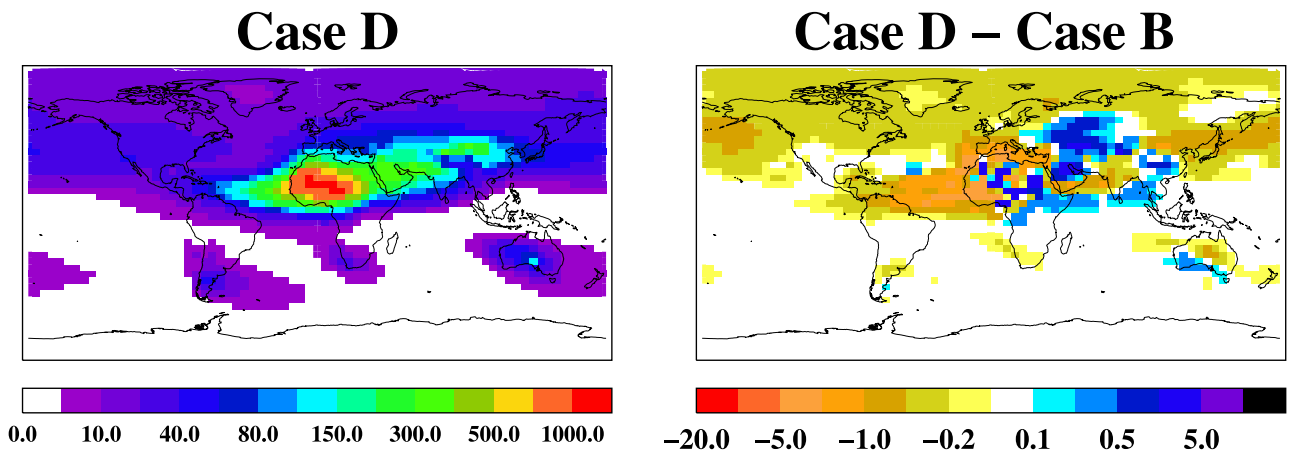

Figure 8. (left) Annual mean column load of dust in experiment case d and (right) the difference in dust load between case d (coated dust) and case b (solubility is set constant to 50%). Units are mg/m^2.

particles can travel large distances, and have a greater chance to collect pollutants on their surface. This causes clay particles to be more soluble. In Table 2 we see that load contributed by the two smallest dust size classes is most sensitive to solubility changes, whereas the two larger size classes are less dependent.

[37] Figure 8 shows the dust load of case d and the difference with respect to case b. Mineral dust aerosol load is reduced in case d over large parts of the Northern Hemisphere and downwind of the Saharan desert, but most important is the reduction of background dust loads far away from the source regions. The difference in total dust load between experiment b and d is only 5% but the difference in clay load is 10%. If we would compare case d to case a, with insoluble dust, the impact of sulfate coating would be much larger. We choose the moderate comparison so as not to overestimate the sulfate coating effect.

[38] *Fan et al.* [2004] found the impact of sulfate coatings on dust hygroscopicity most effective over the east Asian North Pacific. Dust and SO_2 concentrations are high in east Asia, and *Fan et al.* [2004] calculated dust hygroscopicity only dependent on SO_2 abundance. In this study, sulfate coating increases dust deposition in the North Pacific and the Atlantic Ocean. Asian and Saharan dust are affected by hygroscopy changes, because even so SO_2 concentrations are low in the Sahara, sulfate concentrations are high (Figure 3). However, our sulfate loads in Africa are higher as in most models (http://nansen.ipsl.jussieu.fr/AEROCOM/)). In case we overestimate sulfate in northern Africa, we overestimate sulfate coating on Saharan dust as well.

3.3. Climate Impact via Radiative Forcing

[39] The optical and radiative properties are described by K05 and *Koch et al.* [1999] for sulfate aerosols and by Miller et al. (submitted manuscript, 2005) regarding mineral dust. The current radiation scheme has the capability to treat size dependence and relative humidity effects on radiative parameters; however, it assumes the aerosols are externally mixed. In this work we include one additional aerosol type, a particle which has a mineral material core and a shell of sulfate. We expect that the radiative properties of such an internally mixed particle differ from those that are externally mixed. We use a Mie type code to calculate the extinction, single-scattering albedo and asymmetry factor for coated particles [*Mishchenko*, 1990]. The results of this study will be explained in detail in a forthcoming publication (S. E. Bauer et al., Radiative properties of internally mixed ammonium sulfate-nitrate-mineral dust particles, submitted to *Geophysical Research Letters*, 2005). We performed these calculations for size classes between 0.01 and 10 μm and tested the cases where the thickness of the coating ranges between 10 and 100% of the dust particle diameter. The effect of water uptake is included in these results, by performing all radiative calculations under humid conditions, with 75% relative humidity. However, the results of this study are extremely interesting, because the single-scattering albedo of this coated particle is a linear combination of the single-scattering albedo of externally mixed dust and sulfate aerosols, but the asymmetry factor shows a nonlinear response when the shell material is increased. However, if the thickness of the shell material is only 10% or less in comparison to the core material, the radiative parameters, e.g., single-scattering albedo, asymmetry factor and extinction parameter, are very close to the radiative parameters of an externally mixed dust aerosol.

[40] Figure 9 shows the percentage ratio of sulfate thickness material to dust core diameters for the four size classes as used in modelE. 10% sulfate coating is only exceeded in the Arctic on clay particles. However, in this region clay concentrations are very small and the impact of dust on the radiation is very small. In no other region does the sulfate shell material exceed 10% of the core material. Therefore we do not introduce a new aerosol class into the radiation scheme, and it seems appropriate to treat the mixed particles with the same optical parameters as pure dust particles.

[41] Nonetheless, the impact of heterogeneous reactions on the Earth radiation budget is still significant because of the reduction of both externally mixed sulfate aerosols and dust load. Sulfate reflects incoming solar radiation leading to cooling at the Earth surface. In our EXP simulation, the pure sulfate aerosols are reduced, leading to a reduction of the shortwave radiative forcing of sulfate aerosols from -0.56 W/m^2 (K05) to -0.44 W/m^2 (EXP) for present day conditions (see Table 3 and Figure 10). Repeating the same experiments (K05 and EXP) for preindustrial conditions (PI) at 1750, and comparing to the present day (PD), we

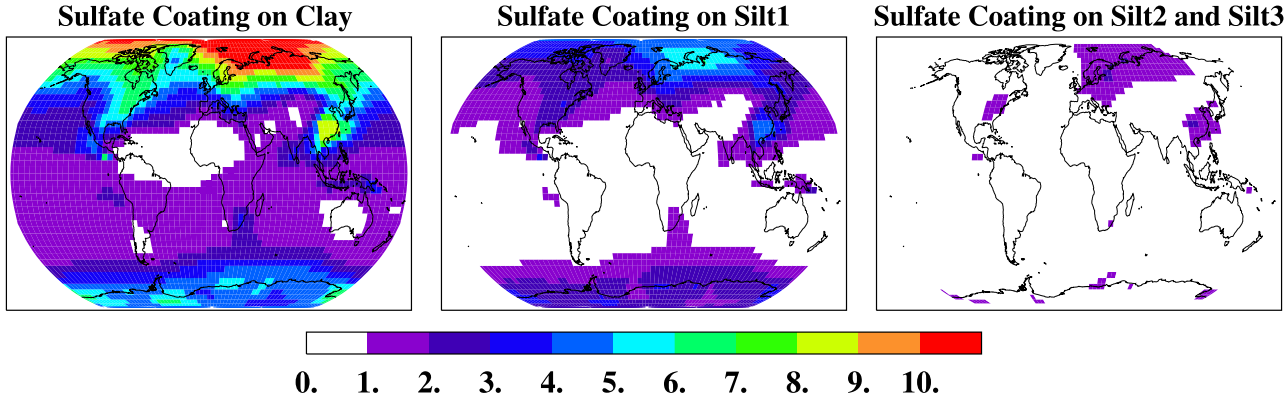

Figure 9. Annual mean ratio of sulfate shell material in relation to dust core material, for the four size classes of mineral dust. Units are in percent.

find the anthropogenic sulfate forcing to be -0.18 W/m^2 and therefore smaller than in the K05, where the anthropogenic sulfate forcing was calculated to be -0.25 W/m^2.

[42] In the case of mineral dust aerosols, the difference in radiative forcing between K05 and EXP results only from the reduced dust load due to increased dust solubility of coated particles. However, the difference in radiative dust forcing between PI and PD (see Figure 10) results from the fact that under PI conditions, there was less sulfate available and therefore the dust particles experienced less coating, which leads to a lower solubility of mineral dust. In this case, we calculate an anthropogenic dust forcing of 0.05 W/m^2. Although, the magnitude of this forcing is extremely uncertain (e.g., as a result of the unknown solubility of non sulfate coated particles) we point out that the sign of this anthropogenic forcing is positive.

[43] In summary, heterogeneous sulfate production on dust particles reduces the radiative cooling effect in two ways; first, by a reduction of pure sulfate particles and second by reducing the mineral dust load.

3.4. Sensitivity Experiments

[44] The results of this paper depend on numerous uncertain factors, for example, the dust and the sulfate aerosol emissions, particle size distributions, transport and removal processes. Sulfate formation on dust depends strongly on the provided dust surface area, SO_2 and O_3 concentrations, relative humidity and the uptake coefficient of SO_2 on the mineral surface. We address uncertainties associated with the uptake rates of SO_2 and the dust size distribution.

[45] To test the influence of uptake rates we perform a set of sensitivity studies where we vary the uptake coefficient, γ_{SO_2}, by 5 orders of magnitude, between 10^{-8} and 10^{-3}. This is sensitivity experiment I, as indicated in Figure 11. In this sensitivity test, γ_{SO_2} is independent of humidity. Figure 11 shows the annual mean total sulfate and pure sulfate concentrations for the sensitivity experiments. The differences of the single experiments are compared to the case without heterogenous sulfate production, K05. For γ_{SO_2} smaller than 10^{-6}, heterogeneous sulfate formation is negligible on the global scale. $\gamma_{SO_2} = 10^{-5}$ leads to no increase in total sulfate mass, but about 20% of pure sulfate mass loss. The most extreme experiment, $\gamma_{SO_2} = 10^{-3}$ has a very strong impact on the global sulfate budget close to 80% of pure sulfate particles are lost, and the total sulfate burden increases by 15%. The experiment discussed in this paper, which depends on humidity (see section 2.1), is indicated by "A" in Figure 11; the total sulfate mass is increased by 3% and pure sulfate aerosols are reduced by 24%.

[46] A second set of sensitivity experiments, noted as II, is performed using the same variations of γ_{SO_2} as explained for sensitivity experiment I, but with a changed size distribution of mineral dust. The total dust emissions are close between I and II, with 1546 Tg/yr for I and 1744 Tg/yr in case II. However, the partitioning between the emitted size classes is different. In case I the following masses are emitted as clay, and silt (0.1–1, 1–2, 2–4, 4–8 μm, respectively): 154, 448, 612 and 532 Tg/yr, and respectively in case II, 322, 474, 474 and 474 Tg/yr. The larger release of smaller particles in case II leads to a much longer overall lifetime of mineral dust, the lifetime is increased from 5.5 to 10.8 days. Therefore in case II, dust particles provide a larger surface area and travel larger distances and have the ability to collect more sulfate material. Figure 11 shows a similar change in SO_4 concentration compared to case I, but a much higher increase in total sulfate mass. The longer lifetime of mineral dust in case II, is associated with a longer lifetime of the sulfate coated on mineral. Again, γ_{SO_2} lower than 10^{-6} has very little impact on the global sulfate cycle, but with increasing uptake rates, heterogeneous sulfate formation increases quickly. In case of the most extreme experiment, $\gamma_{SO_2} = 10^{-3}$, total sulfate mass increases by 40%. When comparing the global budgets of the two A experiments, where γ_{SO_2} was set to either 10^{-3} or 10^{-7}, depending on humidity, we find that heterogeneous sulfate formation increases total sulfate by 3% in case I and by 20% in case II (see Table 1). Therefore the chosen size distribution of the core material, in this study dust is

Table 3. Shortwave Radiative Forcing at TOA

	Sulfate Forcing	Dust Forcing
PD	−0.44	−0.59
EXP – K05	−0.12	−0.05
EXP: PD – PI	−0.18	+0.05
K05: PD – PI	−0.25	-

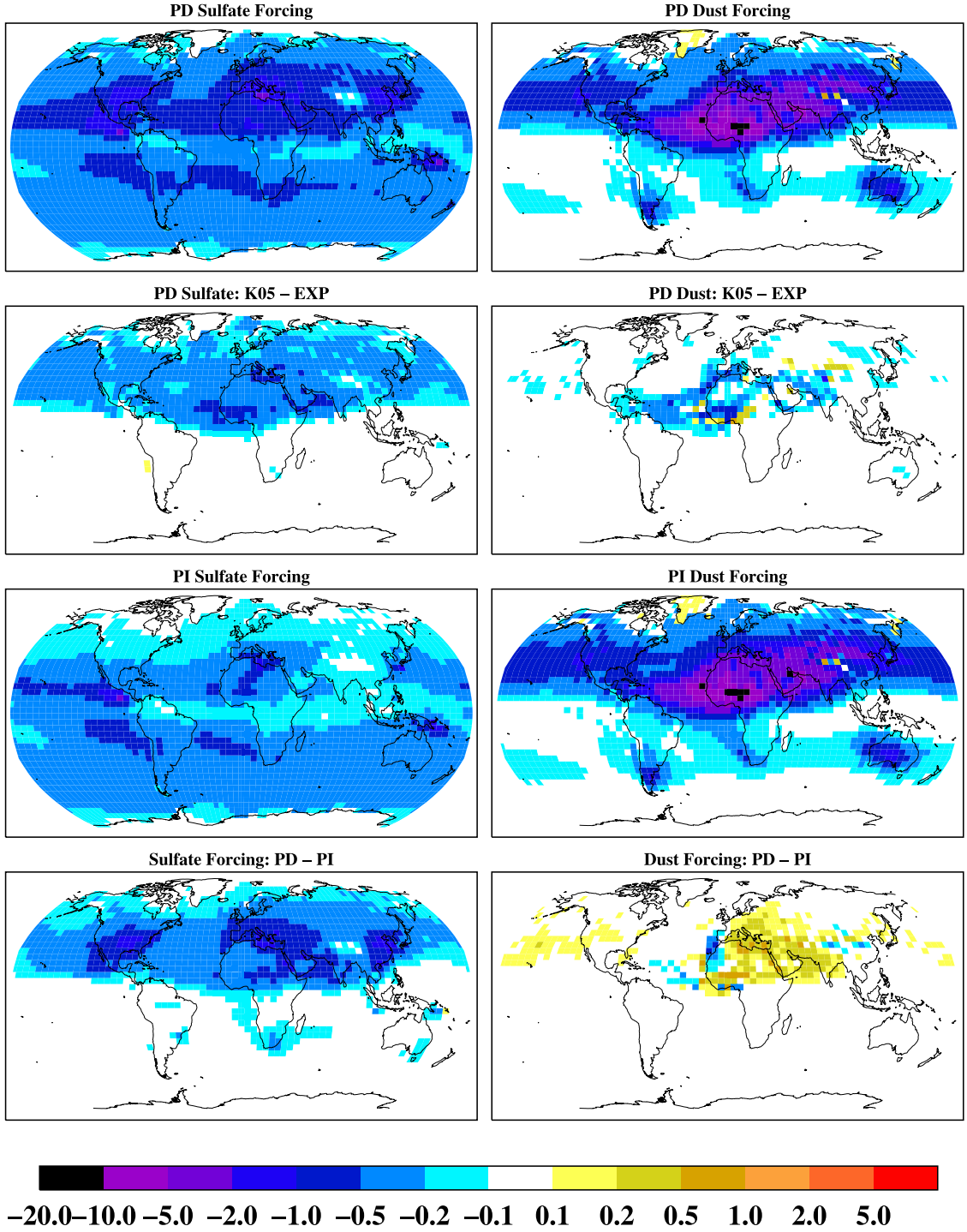

Figure 10. Annual mean shortwave TOA radiative forcing. (left) Contribution of sulfate and (right) Contribution of dust forcing. The uppermost row shows forcing for present-day (PD) conditions. The second row shows the difference in forcing between EXP and K05 (K05 – EXP) for PD. The third row shows preindustrial (PI) forcing, and the fourth row shows the difference between PD and PI. Units are W/m^2.

extremely important for heterogeneous surface reaction rates.

4. Summary and Conclusions

[47] This paper discusses an extension of the sulfate cycle in the new version of the GISS climate model, modelE, compared to a version described by K05. Surface reactions on mineral dust particles allow the formation of an internally mixed sulfate–mineral dust particle. The global sulfate cycle is influenced by this heterogeneous sulfate formation, which reduces SO_2 concentrations, increases total sulfate mass, and reduces externally mixed sulfate aerosols. Coated mineral dust particles are more soluble

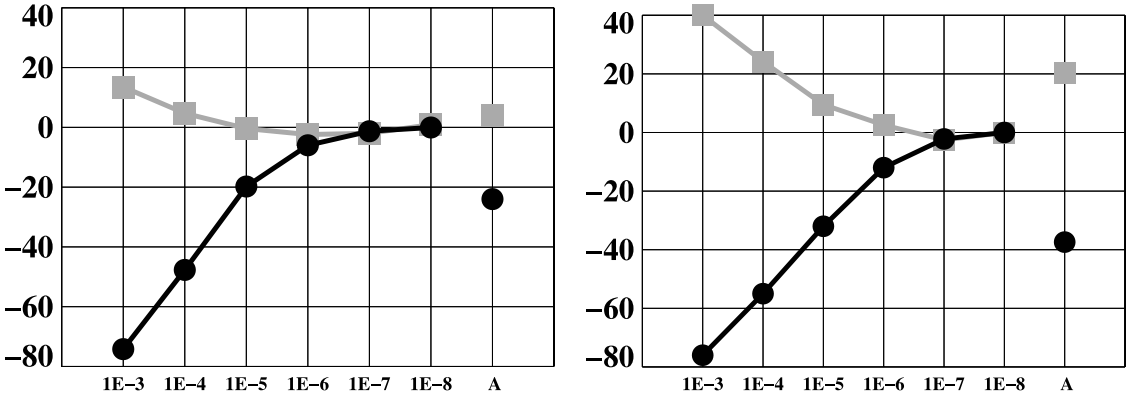

Figure 11. Percentage change in total sulfate mass (grey squares) and pure sulfate aerosol mass (black circles) between the single sensitivity experiments and the base case experiment K05. The *y* axis shows the percentage change, and the *x* axis gives the tested uptake coefficients. "A" indicates the results for the settings of experiment EXP. (left) Sensitivity study I and (right) sensitivity study II.

than noncoated dust, which reduces their lifetime and atmospheric load. The reduction in externally mixed sulfate results in a reduced anthropogenic sulfate radiative forcing. However, at the same time, radiative forcing by mineral dust aerosols becomes less negative because of the higher sulfate coating under PD compared to PI conditions.

[48] The increased load of sulfate mass agrees better with the observations than in K05. The total sulfate mass is only increased by 3%, however, the spatial distribution is very different. The largest impact on sulfate formation is seen over east Asia, where the model shows a doubling of sulfate mass, but still underestimates the observations.

[49] Since EXP performs better overall than K05 (without heterogeneous chemistry), we use this model version in the AEROCOM (http://nansen.ipsl.jussieu.fr/AEROCOM/) intercomparison project.

[50] Comparing our results to prior studies we find a quite large loss of SO_2, about 32% through dust surface reactions. *Liao et al.* [2003] calculated only a 5% loss of SO_2 through heterogeneous sulfate reactions, even though they used much higher uptake rates for SO_2. *Liao et al.* [2003] include in-cloud ozone oxidation in their simulations, which accounts for 20% of the total SO_2 loss in their calculation. We neglect this oxidation pathway and therefore possibly overestimate the heterogeneous SO_2 destruction in clouds. The sulfate simulation by *Liao et al.* [2003] shows a 22% decrease of pure sulfate aerosols and 36% higher global mean mixing ratios of total sulfate near the surface. Our work shows similar results regarding the loss of externally mixed sulfate aerosols but we predict lower increases in total sulfate. However, the results of *Liao et al.* [2003] are in the range of uncertainty we simulated in our sensitivity experiments. *Dentener et al.* [1996] used the same formulation and uptake rates as later used by *Liao et al.* [2003] also using off-line mineral dust, but excluding in-cloud oxidation of ozone and SO_2. We can only compare the annual increase of total sulfate concentrations: their results are in the range of uncertainty of our simulations but regionally quite different; for example, *Dentener et al.* [1996] simulate large impacts over Australia and North America, which we do not simulate. These differences are mainly caused by the different dust simulations.

[51] The sensitivity experiments that are performed to study the robustness of the simulations by varying uptake rates and mineral dust size distributions, show a very strong dependence of heterogenous sulfate formation on these two parameters, which are not very well known. We have used intermediate estimates for those parameters in this study.

[52] Another crucial and relatively unknown factor is the dust solubility. Our study compares the effects of sulfate-coated dust with dust assumed to be 50% soluble. Note that this underestimates the real effect of sulfate on dust, since an assumed nonzero solubility implicitly includes effects of other coatings. For example, nitrate coatings also influence dust solubility. Nitrate precursors are mainly released in industrial and agricultural areas, whereas sulfate precursors are predominantly released in industrial regions. Nitrate coating of dust aerosols might be dominant in different regions and possibly have a larger impact on Saharan dust than sulfate coatings.

[53] In this work we studied the impact and sensitivity of several parameterizations, including solubility, uptake rates and size distributions, on heterogeneous sulfate formation. This list is not complete and many more aspects should be investigated. Especially the large impact of size distribution should be further investigated, including the uncertainties of the modelled dust burden as well. *Zender et al.* [2004] summarized current emission and dust burden of recent simulations and they found emission estimates ranging from 350 to 3000 Tg/yr and burden from 8 to 35.9 Tg. Our dust simulation represents average values of these estimates, but more comparison and validation is needed regarding the size information.

[54] Another important factor is the effect of surface saturation. In this study we did not account for deactivation of the reactive mineral surface after coating already has taken place. Considering the relatively small fraction of sulfate we simulated in comparison to the large dust fraction of the internally mixed particle, surface deactivation process may be negligible in the way this study is carried out. However, laboratory studies show a fast decrease of gaseous uptake rates after initial reactions have taken place. Surface saturation effects need to be investigated in global modeling, especially when more

coating processes, for example including nitrate coatings, are considered.

[55] A further effect on our study might be caused by the coarse resolution of our global simulation. Since mineral dust and SO_2 have widely different source regions, the results will probably depend strongly on the resolution, advection scheme etc. A coarse grid model tends to mix the different air masses more easily and the current model might therefore overestimate the effect of sulfate formation on dust aerosols.

[56] We have also assumed that mixed sulfate dust particles have the same radiative properties as pure mineral dust. Our radiative calculations show that this assumption is valid unless the coating material exceeds 10% of the thickness of the core material diameter. This ratio was not exceeded in our simulation, except at high latitudes in the Northern Hemisphere where dust concentrations are small. However, as we showed in the sensitivity studies, heterogeneous sulfate production is extremely sensitive to our assumptions. For example, a greater clay aerosol load, higher uptake rates, different oxidation mechanisms or solubility assumptions, could possibly lead to a thicker layer of shell material and therefore change significantly the scattering properties of the mixed particles.

[57] As a next step, we plan to use modelE at a higher spatial resolution and simulate measurement campaigns, for example, ACE-Asia and INDOEX, where aerosol chemical composition has been explicitly observed and model composition can be constrained. If we learn that the sulfate deposited on the individual aerosols is much thicker than estimated in the present study, these coated particles need to be treated differently than pure dust particles in the radiation model.

[58] This publication focuses only on the interactions between sulfate and mineral dust. Further heterogenous reactions including sulfate species are important for the total sulfate burden, for example, sulfate heterogeneous chemical reactions on sea salt and soot. Moreover, heterogeneous reactions involving nitrates are important to the dust cycle. Taking into account more heterogenous chemical reaction pathways may lead to a reduced impact of the single (sulfate-dust) heterogeneous reaction.

[59] **Acknowledgments.** We are grateful to Ron Miller for many fruitful discussions and comments on this manuscript. We thank Reha Cakmur and Jan Perlwitz for implementing the dust in modelE and Gavin Schmidt for solving many problems in the model code. We thank Michaele Mishchenko, Sophia Zhang, and Andy Lacis for their assistance with the radiative calculations. Dorothy Koch acknowledges support from the NASA Climate Modeling Program.

References

Andreae, M. O. (1995), Climatic effects of changing atmospheric aerosol levels, in *World Survey of Climatology*, vol. 16, *Future Climates of the World: A Modelling Perspective*, edited by A. Henderson-Sellers, pp. 347–398, Elsevier, New York.

Andres, R. J., and A. D. Kasgnoc (1998), A time-averaged inventory of subaerial volcanic sulfur emissions, *J. Geophys. Res.*, *103*, 25,251–25,262.

Bauer, S. E., Y. Balkanski, M. Schulz, D. A. Hauglustaine, and F. Dentener (2004), Global modelling of heterogeneous chemistry on mineral aerosol surfaces: The influence on tropospheric ozone chemistry and comparison to observations, *J. Geophys. Res.*, *109*, D02304, doi:10.1029/2003JD003868.

Bell, N., D. Koch, and D. T. Shindell (2005), Impacts of chemistry-aerosol coupling on tropospheric ozone and sulfate simulations in a general circulation model, *J. Geophys. Res.*, *110*, D14305, doi:10.1029/2004JD005538.

Brook, R. D., J. Brook, B. Urch, R. Vincent, S. Rajagopalan, and S. V. Silverman (2002), Inhalation of fine particulate air pollution and ozone causes acute arterial vasoconstriction in healthy adults, *Circulation*, *105*, 1534–1536.

Burnett, R. T., S. Cakmak, J. Brook, and D. Krewski (1997), The role of particulate size and chemistry in the association between summertime ambient air pollution and hospitalization for cardio-respiratory diseases, *Environ. Health Perspect.*, *105*, 614–620.

Cakmur, R., R. L. Miller, and O. Torres (2004), Incorporating the effect of small-scale circulations upon dust emission in an atmospheric general circulation model, *J. Geophys. Res.*, *109*, D07201, doi:10.1029/2003JD004067.

Chapman, S., and T. G. Cowling (1970), *The Mathematical Theory of Nonuniform Gases*, Cambridge Univ. Press, New York.

Davis, E. J. (1983), Transport phenomena with single aerosol particles, *Aerosol Sci. Technol.*, *2*, 121–144.

Dentener, F. J., G. R. Carmichael, Y. Zang, J. Lelieveld, and P. J. Crutzen (1996), Role of mineral aerosol as a reactive surface in the global troposphere, *J. Geophys. Res.*, *101*, 22,869–22,889.

Dibb, J. E., R. W. Talbot, G. Seid, C. Jordan, E. Scheuer, E. Atlas, N. J. Blake, and D. R. Blake (2002), Airborne sampling of aerosol particles: Comparison between surface sampling at Christmas Island and P-3 sampling during PEM-Tropics B, *J. Geophys. Res.*, *108*(D2), 8230, doi:10.1029/2001JD000408. [printed *108*(D2), 2003]

Fan, S. M., L. W. Horowitz, H. Levy, and W. J. Moxim (2004), Impact of air pollution on wet deposition of mineral dust aerosols, *Geophys. Res. Lett.*, *31*, L02104, doi:10.1029/2003GL018501.

Fuchs, N. A., and A. G. Sutugin (1970), *Highly Dispersed Aerosols*, 105 pp., Elsevier, New York.

Ginoux, P., M. Chin, I. Tegen, J. M. Prospero, B. Holben, O. Dubovik, and S.-J. Lin (2001), Sources and distributions of dust aerosols simulated with the GOCART model, *J. Geophys. Res.*, *106*, 20,225–20,273.

Ginoux, P., J. M. Prospero, O. Torres, and M. Chin (2005), Long-term simulation of global dust distribution with the GOCART model: Correlation with North Atlantic Oscillation, *Environ. Modell. Software*, *19*(2), 113–128.

Graf, H.-F., J. Feichter, and B. Langmann (1997), Volcanic sulfur emissions: Estimates of source strength and its contribution to the global sulfate distribution, *J. Geophys. Res.*, *102*, 10,727–10,738.

Halmer, M. M., H.-U. Schminke, and H.-F. Graf (2002), The annual volcanic gas input into the atmosphere, in particular into the stratosphere: A global data set for the past 100 years, *J. Volcanol. Geotherm. Res.*, *115*, 511–528.

Hansen, J., et al. (2005), Efficacy of climate forcings, *J. Geophys. Res.*, doi:10.1029/2005JD005776, in press.

Hoell, J. M., D. D. Davis, S. C. Liu, R. E. Newell, H. Akimoto, R. J. McNeal, and R. J. Bendura (1997), The Pacific Exploratory Mission–West Phase B: February–March 1994, *J. Geophys. Res.*, *102*, 28,223–28,240.

Huebert, B. J., T. Bates, P. B. Russell, G. Shi, Y. J. Kim, K. Kawamura, G. Carmichael, and T. Nakajima (2003), An overview of ACE-Asia: Strategies for quantifying the relationships between Asian aerosols and their climatic impacts, *J. Geophys. Res.*, *108*(D23), 8633, doi:10.1029/2003JD003550.

Jacob, D. J., J. Crawford, M. Kleb, V. S. Connors, R. J. Bendura, J. L. Raper, G. W. Sachse, J. C. Gille, L. Emmons, and C. L. Held (2003), Transport and Chemical Evolution Over the Pacific (TRACE-P) aircraft mission: Design, execution, and first results, *J. Geophys. Res.*, *108*(D20), 9000, doi:10.1029/2002JD003276.

Jordan, C. E., J. Dibb, B. E. Anderson, and H. E. Fuelberg (2003), Uptake of nitrate and sulfate on dust aerosols during TRACE-P, *J. Geophys. Res.*, *108*(D21), 8817, doi:10.1029/2002JD003101.

Kettle, A. J., et al. (1999), A global database of sea surface dimethylsulfide (DMS) measurements and a procedure to predict sea surface DMS as a function of latitude, longitude and month, *Global Biogeochem. Cycles*, *13*, 394–444.

Koch, D. (2001), Transport and direct radiative forcing of carbonaceous and sulfate aerosols in the GISS GCM, *J. Geophys. Res.*, *106*, 20,311–20,332.

Koch, D., and J. Hansen (2005), Distant origins of arctic black carbon: A GISS ModelE experiment, *J. Geophys. Res.*, *110*, D04204, doi:10.1029/2004JD005296.

Koch, D., D. Jacob, I. Tegen, D. Rind, and M. Chin (1999), Tropospheric sulfur simulation and sulfate direct radiative forcing in the Goddard Institute for Space Studies general circulation model, *J. Geophys. Res.*, *104*, 23,799–23,822.

Lammel, G., and T. Novakov (1995), Water nucleation properties of carbon black and diesel soot particles, *Atmos. Environ.*, *29*, 813–823.

Levin, Z., E. Ganor, and V. Gladstein (1996), The effect of desert particles coated with sulfate on rain formation in the eastern Mediterranean, *J. Appl. Meteorol.*, *35*, 1511–1523.

Liao, H., P. J. Adams, S. H. Chung, J. H. Seinfeld, L. J. Mickley, and D. J. Jacob (2003), Interactions between tropospheric chemistry and aerosols in a unified general circulation model, *J. Geophys. Res.*, *108*(D1), 4001, doi:10.1029/2001JD001260.

Lohmann, U., and J. Feichter (1997), Impact of sulfate aerosols on albedo and lifetime of clouds: A sensitivity study with the ECHAM4 GCM, *J. Geophys. Res.*, *102*, 13,685–13,700.

Maahs, H. G. (1983), Kinetics and mechanism of the oxidation os S (IV) by ozone in aqueous solution with particular reference to SO_2 conversion in nonurban tropospheric clouds, *J. Geophys. Res.*, *88*, 10,721–10,732.

Menon, S., A. D. DelGenio, D. Koch, and G. Tselioudis (2002), GCM simulations of the aerosol indirect effect: Sensitivity to cloud parameterization and aerosol burden, *J. Atmos. Sci.*, *59*, 692–713.

Mishchenko, M. (1990), Expansion of scattering matrix in generalized spherical harmonics for radially inhomogeneous spherical particles, *Kinematics Phys. Celestial Bodies*, *6*, 93–95.

Nightingale, P., G. Malin, C. S. Law, A. J. Watson, P. S. Liss, M. I. Liddicoat, J. Boutin, and R. C. Upstill-Goddard (2000), In situ evaluation of air-sea exchange parameterizations using novel conservative and volatile tracers, *Global Biogeochem. Cycles*, *14*, 373–387.

Ooki, A., and M. Uematsu (2005), Chemical interactions between mineral dust particles and acid gases during Asian dust events, *J. Geophys. Res.*, *110*, D03201, doi:10.1029/2004JD004737.

Prather, M. J. (1986), Numerical advection by conservation of second order moments, *J. Geophys. Res.*, *91*, 6671–6680.

Prospero, J. M., P. Ginoux, O. Torres, S. E. Nicholson, and T. E. Gill (2002), Environmental characterization of global sources of atmospheric soil dust identified with the NIMBUS 7 Total Ozone Mapping Spectrometer (TOMS) absorbing aerosol product, *Rev. Geophys.*, *40*(1), 1002, doi:10.1029/2000RG000095.

Putaud, J.-P., R. V. Dingenen, A. Dell'Acqua, F. Raes, E. Matta, S. Decesari, M. C. Facchini, and S. Fuzzi (2004), Size-segregated aerosol mass closure and chemical composition in Monte Cimone (I) during MINATROC, *Atmos. Chem. Phys.*, *4*, 889–902.

Savoie, D., and J. Prospero (1982), Particle size distribition of nitrate and sulfate in the marine atmosphere, *Geophys. Res. Lett.*, *9*, 1207–1210.

Savoie, D., J. Prospero, and E. Saltzman (1989), Non-sea-salt sulfate and nitrate in trade wind aerosols at Barbados: Evidence for long-range transport, *J. Geophys. Res.*, *94*, 5069–5080.

Savoie, D. L., J. M. Prospero, R. Arimoto, and R. A. Duce (1994), Non-sea-salt sulfate and methanesulfonate at American Samoa, *J. Geophys. Res.*, *99*, 3587–3596.

Schmidt, G. A., et al. (2005), Present day atmospheric simulations using GISS ModelE: Comparison to in-situ, satellite and reanalysis data, *J. Clim.*, in press.

Shure, K., M. Andreae, and R. Rosset (1995), Biogenic sulfur emissions and aerosols over the tropical South Atlantic: 2. One-dimensional simulation of sulfur chemistry in the marine boundary layer, *J. Geophys. Res.*, *100*, 11,323–11,334.

Sievering, H., J. Cainey, M. Harvey, J. McGregor, S. Nichol, and P. Quinn (2004), Aerosol non-sea-salt sulfate in the remote marine boundary layer under clear-sky and normal cloudiness conditions: Ocean-derived biogenic alkalinity enhances sea-salt sulfate production by ozone oxidation, *J. Geophys. Res.*, *109*, D19317, doi:10.1029/2003JD004315.

Tang, Y., et al. (2004), Impacts of dust on regional tropospheric chemistry during the ACE-Asia experiment: A model study with observations, *J. Geophys. Res.*, *109*, D19S21, doi:10.1029/2003JD003806.

Trochkine, D., Y. Iwasaka, A. Matsuki, M. Yamada, Y.-S. Kim, T. Nagatani, D. Zhang, G.-Y. Shi, and Z. Shen (2003), Mineral aerosol particles collected in Dunhuang, China, and their comparison with chemically modified particles collected over Japan, *J. Geophys. Res.*, *108*(D23), 8642, doi:10.1029/2002JD003268.

Ullerstam, M., R. Vogt, S. Langer, and E. Ljungström (2002), The kinetics and mechnism of SO_2 oxidation by O_3 on mineral dust, *Phys. Chem. Chem. Phys.*, *4*, 4694–4699.

Usher, C. R., H. Al-Hosney, S. Carlos-Cuellar, and V. H. Grassian (2002), A laboratory study of the heterogeneous uptake and oxidation of sulfur dioxide on mineral dust particles, *J. Geophys. Res.*, *107*(D23), 4713, doi:10.1029/2002JD002051.

Usher, C. R., A. E. Michel, and V. H. Grassian (2003), Reactions on mineral dust, *Chem. Rev.*, *103*, 4883–4939.

Wyslouzil, B. E., K. L. Carleton, D. M. Sonnenfroh, W. T. Rawlins, and S. Arnold (1994), Observation of hydration of single, modified carbon aerosols, *Geophys. Res. Lett.*, *21*, 2107–2110.

Zender, C. S., R. L. Miller, and I. Tegen (2004), Quantifying mineral dust mass budgets: Systematic terminology, constraints, and current estimates, *Eos Trans. AGU Electron. Suppl.*, *85*(48), 30 Nov. (Available at http://www.agu.org/eos_elec/000790e.php)

Zhang, D., and Y. Iwasaka (2004), Size change of Asian dust particles caused by sea salt interactions: Measurements in southwestern Japan, *Geophys. Res. Lett.*, *31*, L15102, doi:10.1029/2004GL020087.

Zhang, D., G. Shi, Y. Iwasaka, and M. Hu (2000), Mixture of sulfate and nitrate in coastal atmospheric aerosols: Individual particle studies in Qingdao (36°04′N, 120°21′E), China, *Atmos. Environ.*, *34*, 2669–2679.

Zhuang, H. C., C. K. Chan, M. Fang, and A. S. Wexler (1999), Formation of nitrate and non-sea-salt sulfate on coarse particles, *Atmos. Environ.*, *33*, 4223–4233.

S. E. Bauer and D. Koch, NASA Goddard Institute for Space Studies, 2880 Broadway, New York, NY 10025, USA. (sbauer@giss.nasa.gov)